Anisotropic Magnetized White Dwarfs: Unifying Under- and Overluminous Peculiar and Standard Type Ia Supernovae

Debabrata Deb[1] , Banibrata Mukhopadhyay[1] , and Fridolin Weber[2,3]
[1] Department of Physics, Indian Institute of Science, Bangalore 560012, India; debabratadeb@iisc.ac.in, bm@iisc.ac.in
[2] Department of Physics, San Diego State University, San Diego, CA 92182, USA
[3] Center for Astrophysics and Space Sciences, University of California at San Diego, La Jolla, CA 92093, USA; fweber@sdsu.edu

Abstract

Ever since the observation of peculiar overluminous Type Ia supernovae (SNeIa), exploring possible violations of the canonical Chandrasekhar mass limit (CML) has become a pressing research area of modern astrophysics. Since its first detection in 2003, more than a dozen of peculiar overluminous SNeIa has been detected, but the true nature of the underlying progenitors is still under dispute. Furthermore there are also underluminous SNeIa whose progenitor masses appear to be well below the CML (sub-Chandrasekhar progenitors). These observations call into question how sacrosanct the CML is. We have shown recently in Paper I that the presence of a strong magnetic field, the anisotropy of dense matter, as well as the orientation of the magnetic field itself significantly influence the properties of neutron and quark stars. Here, we study these effects for white dwarfs (WDs), showing that their properties are also severely impacted. Most importantly, we arrive at a variety of mass–radius relations of WDs that accommodate sub- to super-Chandrasekhar mass limits. This urges caution when using WDs associated with SNeIa as standard candles.

1. Introduction

Recently, Deb et al. (2021, hereinafter referred to as Paper I) initiated the exploration of effects of anisotropy on strongly magnetized compact stars in general relativity. They showed in their work that not only the presence of a strong magnetic field and anisotropy, but also the orientation of the magnetic field itself, significantly influence the physical properties of stars. They further showed that static equilibrium is not achieved unless both the local matter anisotropy effects and the anisotropy effects caused by a strong magnetic field are considered. Paper I showed that for a transversely oriented magnetic field, the stellar mass increases with increasing field strength, which however is opposite to a radially oriented field. Based on a detailed exploration, it was argued that massive neutron and strange quark stars of masses more than $2.5\,M_\odot$ are possible. The authors also briefly touched upon the possible violation of the Chandrasekhar mass limit (CML), based on this idea. Chandrasekhar (1931, 1935) first introduced the idea of the possible limiting mass for WDs in his celebrated works, where he predicted that beyond $\sim 1.4\,M_\odot$ no nonrotating and nonmagnetized carbon–oxygen (C–O) white dwarfs (WDs) exist. This critical mass limit is famously known as the CML for WDs.

In this article, we explore in detail the effects of the abovementioned anisotropy due to high magnetic field strengths as well as matter properties in WDs. Stable equilibrium configurations of WDs are achieved due to the repulsive electron degeneracy pressure, which counterbalances the inward gravitational pull. When WDs gain mass (say, via

mass accretion from companion stars) and exceed a certain critical mass limit, the inward gravitational force overpowers the repulsive force of the degenerate electrons, which leads to a situation where fusion reactions are initiated. Within a few seconds, runaway reactions set in to unbind a considerable amount of WD matter through an explosion which releases an enormous amount of energy, $\sim 10^{51}$ erg, known as a Type Ia supernova (SNIa). This violent cosmic event ensures a generally complete disruption of WDs without leaving behind any stellar remnant. However, recently another class of supernovae related to WDs, named Type Iax supernovae, has been observed which look similar to SNeIa but are much fainter. In the case of Type Iax supernovae, the progenitors may partially survive the explosions and move away at high kick velocities (Vennes et al. 2017).

Type Ia supernovae (SNeIa) manifest a specific set of relations between intrinsic luminosity, color, and light-curve width (Phillips 1993; Goldhaber et al. 2001). Such standard and stable physical features of SNeIa help astronomers to use them as standard candles to accurately measure the distances to their host galaxies. The variation of the brightness of SNeIa with the distance is a key technique used to measure cosmological parameters. In fact, the pioneering observation of the accelerated expansion of the universe, which confirms the probable role of dark energy behind this cosmic phenomenon, was inferred from the consideration of SNIa to be a standard candle (Riess et al. 1998; Perlmutter et al. 1999). However, in recent years, a series of observations of several peculiar overluminous SNeIa, such as *SN 2003cv* (Howell et al. 2006), *SN 2007fg* (Scalzo et al. 2010), *SN 2009if* (Taubenberger et al. 2011), and *SN 2013dc* (Cao et al. 2016), constitute a serious setback to the generally accepted standard candle concept, as they are best explained by massive progenitor WDs having mass beyond the standard CML. As SNeIa are mainly powered

by the radioactive decay of ^{56}Ni, to explain 2.2 times overluminous SN 2003cv, Howell et al. (2006) predicted that it requires $\sim 1.3\,M_\odot$ of ^{56}Ni, which leads to a possible progenitor WD with a mass of $\sim 2.1\,M_\odot$, popularly known as a super-Chandrasekhar progenitor WD (SCPWD). Later, researchers discovered the overluminous SN 2009if having a high-mass SCPWD as $\sim 2.8\,M_\odot$.

Due to peculiar features of these overluminous SNeIa, they immediately attracted the attention of researchers who came up with two possible explanations such as (i) mergers of massive WDs (Iben & Tutukov 1984; Hicken et al. 2007) and (ii) explosions of rapidly rotating WDs (Howell et al. 2006; Boshkayev et al. 2013; Branch 2006). In a double C–O WD system, one star accretes mass from the companion C–O rich WD. In the accreting WD, the ignition of carbon burning starts due to the heating of the outer layer if the accretion rate exceeds the critical limit of $2.7 \times 10^{-6}\,M_\odot\,\mathrm{yr}^{-1}$ (Nomoto & Iben 1985; Kawai et al. 1987). The final stage of the accreting WD depends on whether carbon ignition is at the center or in the envelope of the star. If carbon ignition starts at the stellar core of a WD, it leads to a SNIa explosion. On the other hand, ignition in the stellar envelope leads to the propagation of a deflagration flame toward the center and the immediate conversion of a C–O WD to an O–Ne–Mg WD (Saio & Nomoto 1985, 1998; Timmes et al. 1994), which finally collapses into an ultra-dense neutron star (Nomoto 1984, 1987; Nomoto & Kondo 1991). In both cases, the double degenerate scenario does not lead to a SNIa explosion that could explain a $2.8\,M_\odot$ SCPWD. In fact, numerical simulations of massive WD mergers indicate the collapse of an accreting WD to a neutron star due to off-center carbon burning (Saio & Nomoto 2004; Martin et al. 2006). On the other hand, Chen & Li (2009) showed that a differentially rotating accreting WD in close vicinity to its companion star cannot exceed a mass of $1.7\,M_\odot$. Therefore, it is clear that the above discussed two competing scenarios of SNIa progenitors fail to explain high-mass SCPWDs.

Later, Mukhopadhyay and collaborators (Das & Mukhopadhyay 2012a; Kundu & Mukhopadhyay 2012) introduced a magnetic WD model where they suitably explained SCPWDs. This model considers high magnetic fields within the stellar structure having Landau levels in the plane perpendicular to the axis of the magnetic field and is therefore able to explain highly massive SCPWDs with masses of $\sim 2.6\,M_\odot$ (Das & Mukhopadhyay 2013a). Das & Mukhopadhyay (2014a) also proposed that if the strong magnetic field within the magnetized WDs (hereinafter B-WDs) is fluctuating/tangled at a length scale larger than the quantum length scale, the average magnetic field and corresponding magnetic pressure could be considerably smaller than the matter pressure, which is however modified by the Landau quantization. The degree of Landau quantization influences the quasi-equilibrium state of highly magnetized B-WDs, which modifies the matter pressure that counterbalances the inward gravitational pull. Hence, the mass–radius relation of B-WDs deviates more and more from the CML the longer the accretion of the mass continues (Das & Mukhopadhyay 2012b, 2013a; Das et al. 2013b). The mass loading onto B-WDs leads to an increase in central density which contracts their size (Cumming 2002). As a consequence, the central magnetic field of B-WDs may increase accordingly due to the magnetic flux freezing theorem.

Interestingly, by applying the varying accretion rate scenario, Das et al. (2013b) argued that a $0.2\,M_\odot$ WD with a $10^9\,\mathrm{G}$ surface magnetic field (B_s) turns into a super-Chandrasekhar B-WD (SCBWD) within 2×10^7 yr. Mukhopadhyay and his group over the years have been attempting to develop a more sophisticated and generalized model that would explain the complex astrophysical situations for SCBWDs realistically by accounting for the general relativistic effect, differential rotation, variations of the magnetic fields and geometry, the Landau quantization, thermal luminosity, deviations from spherical symmetry, etc.; see Das & Mukhopadhyay (2014b, 2015a), Subramanian & Mukhopadhyay (2015), Mukhopadhyay & Rao (2016), Mukhopadhyay et al. (2017), Bhattacharya et al. (2018), Gupta et al. (2020), and Mukhopadhyay et al. (2021). They (Kalita & Mukhopadhyay 2019; Kalita et al. 2020) also showed how it is possible to detect SCPWDs directly via continuous gravitational-wave astronomy in the various upcoming space-based detectors, such as the Deci-hertz Interferometer Gravitational Wave Observatory (DECIGO), Laser Interferometer Space Antenna (LISA), and Big Bang Observer (BBO). The idea of SCBWDs proposed by Mukhopadhyay and his group has also been explored and confirmed by different independent research works, such as by Federbush et al. (2015), Franzon & Schramm (2015, 2017), Moussa (2017), Shah & Sebastian (2017), Sotani & Tatsumi (2017), and Roy et al. (2019).

As described in Paper I, Bowers & Liang (1974) strongly argued against the oversimplistic assumption that compact stars are entirely made up of an isotropic perfect fluid. They generalized the Tolman–Oppenheimer–Volkoff (TOV) equation (Tolman 1939; Oppenheimer & Volkoff 1939), which describes the structure of spherically symmetric stars, to systems where pressure is anisotropic. They also showed that the inclusion of local anisotropy leads to nonnegligible effects on the properties of stars, such as the total mass, radius, density, and surface redshift. Interestingly, the spontaneous creation of strong magnetic fields within a compact star breaks the spatial rotational symmetry, $\mathcal{O}(3)$, which leads to pressure anisotropy within the stellar structure (Ferrer et al. 2010; Isayev & Yang 2011, 2012). As to the other origin of anisotropy, it is the consequence of the cooling process of WDs, which takes almost the entire time of its evolutionary stage, lasting for nearly 10 Gyr. During the cooling at low temperatures, a first-order fluid–solid transition occurs in the WD's dense plasma, as accurately predicted by Kirzhnits (1960), Abrikosov (1960), and Salpeter (1961) in the early 1960s. Later, Stevenson (1980) showed via his proposed phase diagram that carbon and oxygen are immiscible in the solid phase, which was confirmed by Garcia-Berro et al. (1988). Nag & Chakrabarty (2000) in their study discussed the cooling of WDs via condensation of a Bose gas leading to a first-order phase transition. They also predicted that the cores of massive WDs are actually Bose condensed and made of crystalline normal crustal matter, which is comparable to the ultra-dense neutron star structure, including a superfluid core and normal neutron matter crust.

While one may find several works treating magnetized nonspherical stars in general relativity with publicly available numerical codes (XNS and LORENE) or the perturbative approach solving the Einstein–Maxwell field equations, with toroidal, poloidal, or mixed field geometries, (see, e.g., Bocquet et al. 1995; Konno et al. 1999; Cardall et al. 2001; Oron 2002; Ioka & Sasaki 2004; Kiuchi & Kotake 2008; Kiuchi et al. 2009;

Yasutake et al. 2010; Frieben & Rezzolla 2012; Yoshida et al. 2012; Das & Mukhopadhyay 2015a; Subramanian & Mukhopadhyay 2015; Kalita & Mukhopadhyay 2019; Kalita et al. 2020), none of them include the effects of anisotropy, making them incomplete. Importantly, in Paper I we showed that it is essential to consider the effective anisotropy, both due to the fluid and the field, as it has a notable impact on the structure of magnetized stars. Therefore, in the light of the above discussions, in this work, we include the pressure anisotropy in order to obtain a generalized picture of the structure of WDs.

Recently, Chowdhury & Sarkar (2019) proposed an anisotropic, spherically symmetric model for nonmagnetized WDs in the framework of scalar–tensor theories of gravity. On the other hand, Chu et al. (2014) showed that the magnetic field strength and its orientation significantly affect the maximum mass of stars. Although they attempted to consider magnetic field orientations, the effects of the magnetic field orientation and of the pressure anisotropy are not explicitly included in the TOV equation used in their model, which was rectified in Paper I. Hence, in the present work, we include both the magnetic field strength and its orientation in the TOV equation to achieve a more complete description of the effects of the magnetic fields and anisotropy on the properties of WDs. Like in Paper I, we denote the orientation of the magnetic fields along the radial direction as the radial orientation (RO) and their orientation along the orthogonal to the radial direction (say along the θ- or ϕ-directions) as the transverse orientation (TO). Importantly, we further show that the stability of B-WDs is not achieved unless we consider the anisotropy of the system arising from the combined effects of (i) anisotropy due to strong magnetic fields and (ii) anisotropy of the system fluid.

We organize this paper as follows. In Section 2 we discuss the basic formalisms for B-WDs and show that it is important to consider anisotropy due to both the fluid and field. In Section 3 we discuss the results and show the effects of anisotropy, magnetic fields, and their orientations on the different physical properties of WDs. Important concluding remarks are provided in Section 4.

2. Basic Formalisms for B-WDs

The formalism of this paper is identical to the one used in Paper I, where stars are assumed to be approximately spherically symmetric. It has already been shown that toroidally dominated, stable magnetized WDs maintain their spherical symmetric shape to a very good approximation (Das & Mukhopadhyay 2015a; Subramanian & Mukhopadhyay 2015; Kalita & Mukhopadhyay 2019). Hence, our restriction to spherically symmetric magnetized stars is not ad hoc, since highly magnetized stars are already shown to be toroidally dominated (Wickramasinghe et al. 2014; Quentin & Tout 2018). Moreover, the chosen strength of the magnetic field does not practically bring in any effects due to Landau quantization, see Das & Mukhopadhyay (2014a, 2014b, 2015a). This in turn also assures minimal or almost no effect on the symmetric structure of B-WDs. Note also that the magnetization has a negligible effect due to the magnetic field strength considered in this paper. The contribution of magnetization to the pressure is at least an order of magnitude smaller than the magnetic field pressure, i.e., $B^2/8\pi$. In fact, the minor effect of magnetization to pressure has been already explored in a few earlier works, see, e.g., Ferrer et al. (2010) and Sinha et al. (2013).

The effective contributions from the matter (ρ) and the magnetic field (ρ_B) lead to the system density ($\tilde{\rho}$), given by

$$\tilde{\rho} = \rho + \frac{B^2}{8\pi}. \tag{1}$$

The system pressure along the direction to the magnetic field is represented as parallel pressure and takes the form, according to magnetic field orientations, of

$$p_\parallel = \begin{cases} p_r - \dfrac{B^2}{8\pi}, & \text{for RO,} \\[2mm] p_t - \dfrac{B^2}{8\pi}, & \text{for TO.} \end{cases} \tag{2}$$

Similarly, the system pressure that aligns perpendicular to the magnetic fields is defined as transverse pressure and, based on the magnetic field orientations, takes the form

$$p_\perp = \begin{cases} p_t + \dfrac{B^2}{8\pi}, & \text{for RO,} \\[2mm] p_r + \dfrac{B^2}{8\pi}, & \text{for TO.} \end{cases} \tag{3}$$

Based on the TOV equations, as shown in Paper I, and considering the magnetic field orientations, we obtain the essential magnetostatic stellar equations which describe static, spherically symmetric B-WDs, given by

$$\frac{dm}{dr} = 4\pi\left(\rho + \frac{B^2}{8\pi}\right)r^2, \tag{4}$$

$$\begin{cases} \dfrac{dp_r}{dr} = \dfrac{-(\rho + p_r)\dfrac{4\pi r^3\left(p_r - \frac{B^2}{8\pi}\right) + m}{r(r - 2m)} + \frac{2}{r}\Delta}{\left[1 - \dfrac{d}{d\rho}\left(\frac{B^2}{8\pi}\right)\dfrac{d\rho}{dp_r}\right]}, & \text{for RO,} \\[6mm] \dfrac{dp_r}{dr} = \dfrac{-\left(\rho + p_r + \frac{B^2}{4\pi}\right)\dfrac{4\pi r^3\left(p_r + \frac{B^2}{8\pi}\right) + m}{r(r - 2m)} + \frac{2}{r}\Delta}{\left[1 + \dfrac{d}{d\rho}\left(\frac{B^2}{8\pi}\right)\dfrac{d\rho}{dp_r}\right]}, & \text{for TO.} \end{cases} \tag{5}$$

Here we describe the effective anisotropy of the stars with Δ, which depends on the magnetic field orientations $p_t - p_r + \frac{B^2}{4\pi}$ in the case of RO and $p_t - p_r - \frac{B^2}{8\pi}$ for TO (Paper I). Note that the standard form of the TOV equation (Bowers & Liang 1974; Herrera & Barreto 2013) for nonmagnetized, anisotropic stars is retrieved by considering $B = 0$.

If one ignores local anisotropy due to the fluid, i.e., $p_t = p_r$, the right side of Equation (5) diverges at $r = 0$ as the central magnetic field B_c is maximal at around center, which makes isotropic, highly magnetized WDs unstable. Since no exact theoretical form exists in the literature to deal with anisotropy, an approach that serves to avoid this instability has been proposed in Paper I.

In Paper I, we already modeled the effective anisotropy that appeared in the TOV equations, which is the magnetized version of the Bowers–Liang proposal (Bowers & Liang 1974),
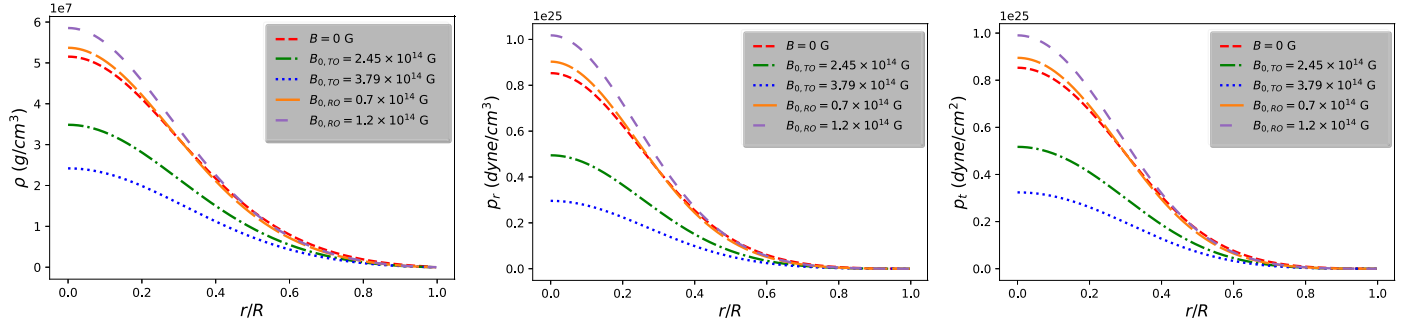
Figure 1. Variation of (a) matter density (ρ; left panel), (b) radial pressure (p_r; middle panel), and (c) tangential pressure (p_t; right panel) with a radial distance r/R of a magnetized 1.3 $M_\odot$ WD. Here and in what follows $\kappa = 0.45$, $\eta = 0.2$, $\gamma = 0.9$, and $B_s = 10^9$ G. The labels RO and TO are explained in the text.

given by

$$
\Delta = \begin{cases} \kappa \dfrac{(\rho + p_r)\left(\rho + 3\,p_r - \frac{B^2}{4\pi}\right)}{\left(1 - \frac{2m}{r}\right)} r^2, & \text{for RO}, \\[4mm] \kappa \dfrac{\left(\rho + p_r + \frac{B^2}{4\pi}\right)\left(\rho + 3\,p_r + \frac{B^2}{2\pi}\right)}{\left(1 - \frac{2m}{r}\right)} r^2, & \text{for TO}, \end{cases}
$$
(6)

where κ is a dimensionless constant that describes the strength of anisotropy within the stellar structure. κ chosen in this work lies well within the permissible range of $\left[-\frac{2}{3}, \frac{2}{3}\right]$ (Silva et al. 2015). Note importantly that $\kappa = 0$ implies that the anisotropy effects due to matter properties and magnetic field both vanish. However, the case of $B = 0$ but $\kappa \neq 0$ implies that only the anisotropy due to the magnetic field vanishes. In this work, we show that highly magnetized WD models that do not account for the combined anisotropic effects of the fluid and field are eliminated as they suffer an instability at the stellar center. Our phenomenological approach offers the best possible way to solve the (magneto-) hydrostatic equilibrium equations, which include anisotropic effects.

To solve the (magneto-) hydrostatic stellar structure (Equations (4) and (5)) from the stellar center to surface, it is required to supply an equation of state (EoS), which connects ρ with p_r, along with the functional form of Δ. In this work we consider an EoS proposed by Chandrasekhar to explain WDs supported by electron degeneracy pressure, given by

$$
p_r = \frac{\pi m_e^4 c^5}{3h^3} [x(2x^2 - 3)\sqrt{x^2 + 1} + 3\,\sinh^{-1}x],
$$
$$
\rho = \frac{8\pi \mu_e m_H (m_e c)^3}{3h^3} x^3,
$$
(7)

where m_e is the mass of an electron, m_H is the mass of a hydrogen atom, h is Planck's constant, μ_e is the mean molecular weight per electron, and $x = p_F/m_e c$ with p_F is the Fermi momentum. For the description of C–O WDs in this work we set $\mu_e = 2$. To solve the coupled nonlinear differential Equations (4) and (5) we consider boundary conditions at (i) the stellar center $m(r)|_{r=0} = 0$ and $\rho(r)|_{r=0} = \rho_c$ and (ii) the stellar surface $\rho(r)|_{r=R} = 0$, which ensures the essential junction condition proposed by O'Brien & Synge (1952) and Robson

(1972), i.e., $p_r = 0$. To describe the exterior spacetime we consider the Schwarzschild metric.

It is generally known that the central magnetic field strength (B_c) is several orders of magnitude higher than B_s (Fujisawa et al. 2012; Das & Mukhopadhyay 2014b; Subramanian & Mukhopadhyay 2015). This phenomenon is due to the presence of a fossil field in the progenitor star, which is supposed to be stronger at the stellar core than at the surface, and the dynamo effect which ensures a strong field at the center (Potter & Tout 2010). This feature is taken into account by adopting the density-dependent magnetic field profile of Paper I, which decreases monotonically inside B-WDs, from its maximum finite value at the center to its minimum value at the surface. This appropriately mimics the spatial dependence of the magnetic field strength. The chosen density-dependent magnetic field profile, which was originally proposed by Bandyopadhyay et al. (1997, 1998) and applied later to WDs by Das & Mukhopadhyay (2014b) and Bhattacharya et al. (2018), is given by

$$
B(\rho) = B_s + B_0 \left[1 - \exp\left\{ -\eta \left(\frac{\rho}{\rho_0} \right)^\gamma \right\} \right],
$$
(8)

where the dimensionless parameters η and γ control how $B(\rho)$ decreases from the center to the surface of a magnetized star. Here, following Bhattacharya et al. (2018) we chose $\rho_0 = 10^9$ g cm^{-3}, $\gamma = 0.9$, and $\eta = 0.1$. We also assume that $B_s = 10^9$ G, which is consistent with the observations made by the Sloan Digital Sky Survey (SDSS; Schmidt et al. 2003; Kepler et al. 2015; Ferrario et al. 2020). Nevertheless, our results are not sensitive to $B_s \lesssim 10^9$ G, as shown previously by, e.g., Das & Mukhopadhyay (2015a) and Gupta et al. (2020).

However, Dexheimer et al. (2017) later proposed that the density-dependent magnetic field strength profile should be polynomial instead of exponential, which we may explore in future works. The validity of Maxwell's equation for this choice of magnetic field profile with respect to the chosen field orientations was discussed in detail in Paper I and thus will not be repeated here.

3. Results and Discussions

Our study reveals that the orientations of magnetic fields (such as RO and TO) significantly affect the structural and interior properties of B-WDs. To feature the combined effects of anisotropy, magnetic fields, and their orientations to the said structural and interior properties, we take a WD candidate with a mass of 1.3 $M_\odot$ and a surface magnetic field of 10^9 G in
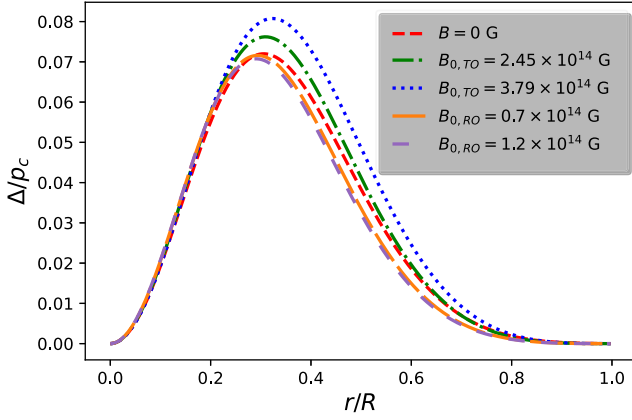
Figure 2. Variation of anisotropy (Δ), normalized to central matter pressure (p_c), as a function of radial distance r/R for a magnetized 1.3 $M_\odot$ WD.

Figure 3. Variation of parallel pressure ($p_\parallel$) and transverse pressure ($p_\perp$) with system density ($\tilde{\rho}$), normalized to the central system density ($\tilde{\rho}_c$) for a magnetized 1.3 $M_\odot$ WD.

Figure 4. Variation of magnetic field strength $B(\rho)$ with radial coordinate r/R for a magnetized 1.3 $M_\odot$ WD.

Figures 1, 2, 3, and 4. Since the effect of the magnetic field on the stellar mass is not same for the RO and TO fields, we choose different B_0 for the TO and RO fields. TO and RO in the subscript of B_0 denote the associated magnetic field orientations. Moreover, the values of the (constant) free parameters have been chosen such that the progenitors of the observed peculiar overluminous SNeIa can be explained.

The profiles for matter density ρ with respect to normalized radial coordinate r/R are shown in the left panel of Figure 1, where R is the radius of WDs. The profiles of the radial pressure p_r and tangential pressure p_t of the matter are shown in the middle and right panels of Figure 1, respectively. Figure 1 shows that ρ, p_r, and p_t have maximum finite values at the stellar center which decrease gradually to reach their minimum values at the surface, which also ensures the physical regularity of the proposed model. It is also evident from Figure 1 that this proposed stellar model is free from a gravitational singularity (or spacetime singularity). In Figure 2 we show the profiles of anisotropy (Δ) in WDs for the TO and RO magnetic fields. One sees that the maximal anisotropic stress inside a TO WD increases with B_0. This is in contrast to RO fields, in which case the maximal anisotropic stress decreases for increasing B_0. Importantly, the anisotropy is zero at the center of the B-WDs, which ensures the consistency of the equilibrium of forces at every interior stellar location, from the center to the surface of the stellar structure. One can see that for the TO fields, in the case of $B_0 = 3.79 \times 10^{14}$ G, the maximum effective anisotropy is $\sim$92% lower in magnitude compared to the matter central pressure p_c which is minuscule to drive the stellar configuration toward nonspherical symmetry.

In Figure 3 we show the combined effects of the magnetic field and its orientation on the parallel pressure $p_\parallel$ and transverse pressure $p_\perp$. One sees that as B_0 increases for the TO fields, the slope of the system pressure profile decreases due to the increase of the size of the star and the decrease of the outward hydrodynamic force (F_h). In contrast, the system pressure profiles stiffen for increasing B_0 in the RO case as the size of the star decreases and F_h gradually increases. Note that at the center and surface of the stars, $p_\parallel$ and $p_\perp$, have the same value, reflecting the consistency of the TOV equation of highly magnetized B-WDs in the present treatment. This was overlooked by almost all the researchers before Paper I. On the other hand, it has already been shown that for toroidal fields B-WDs approximately maintain their spherically symmetric configuration (Das & Mukhopadhyay 2015a; Subramanian &
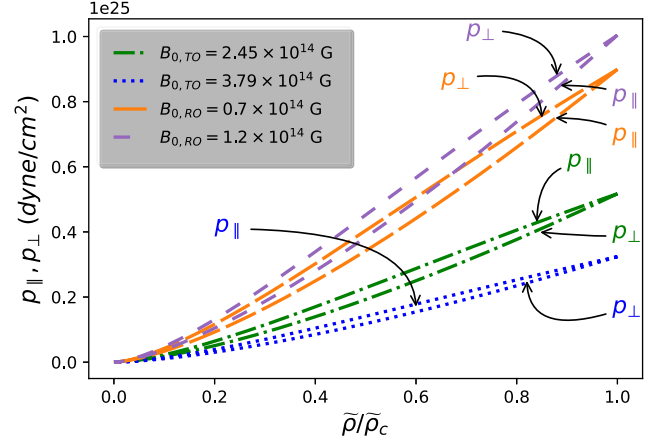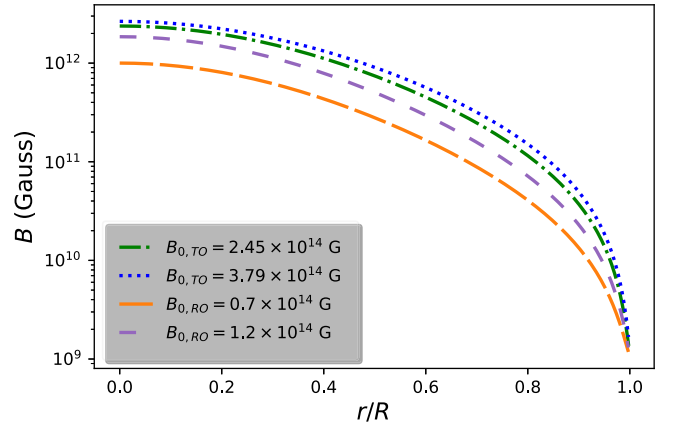
Mukhopadhyay 2015; Kalita & Mukhopadhyay 2019). We show the density-dependent magnetic field profiles for different TO and RO fields in Figure 4 which, as expected, are maximal at the center and decrease gradually within B-WDs to reach their minimum values at the surface.

In Figure 5, we show the mass–radius relations of B-WDs for different B_0, κ, and γ. Our study shows that for TO fields with $B_0 = 3.79 \times 10^{14}$ G, a maximum mass B-WD of 2.8 $M_\odot$ is obtained whose radius is 1457.67 km. For a RO field with $B_0 = 1.2 \times 10^{14}$ G, the maximum mass drops to 1.62 $M_\odot$ and the radius of the WD is 454.67 km, as shown in the left panel of Figure 5. We find for $B_{0,TO} = 3.79 \times 10^{14}$ G that the maximum mass and the corresponding radius of B-WDs increase by $\sim$70% and $\sim$57%, respectively, compared to the nonmagnetized but anisotropic case. For $B_{0,RO} = 1.2 \times 10^{14}$ G, the maximum mass and the corresponding radius decrease by $\sim$2% and $\sim$52%, respectively, compared to the values of nonmagnetized but anisotropic WDs. Note that without considering the magnetic field and incorporating the effects of local anisotropy due to the fluid, it is possible to push the maximum mass of WDs beyond the CML. For example, by considering $\kappa = 2/3$, we obtain a maximum mass for a nonmagnetized but anisotropic WD of 1.81 $M_\odot$. The corresponding radius is 956.08 km. These values are $\sim$29% and $\sim$8%, respectively, higher than the respective values of WDs at the CML. One sees an almost similar trend in the middle panel of Figure 5, which
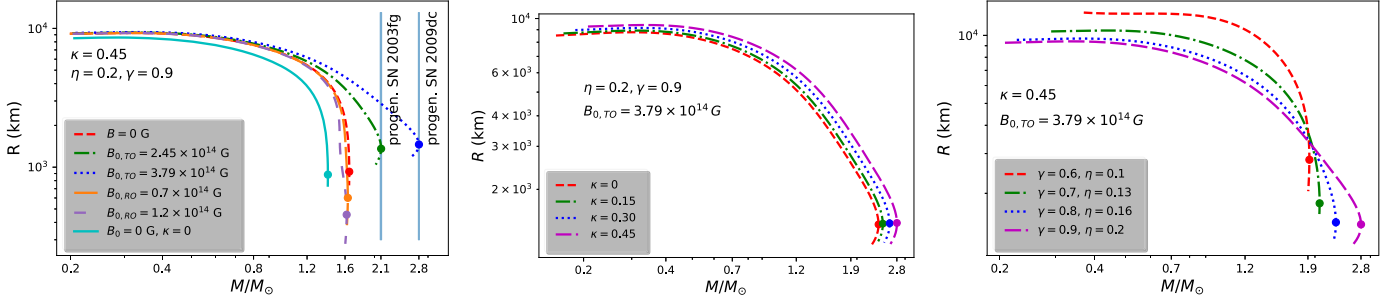
Figure 5. Stellar radius (R) as a function of gravitational mass ($M/M_\odot$) for different (a) B_0 (left panel), (b) κ (middle panel), and (c) η and γ (right panel). Solid circles represent the stars with the maximum possible masses.
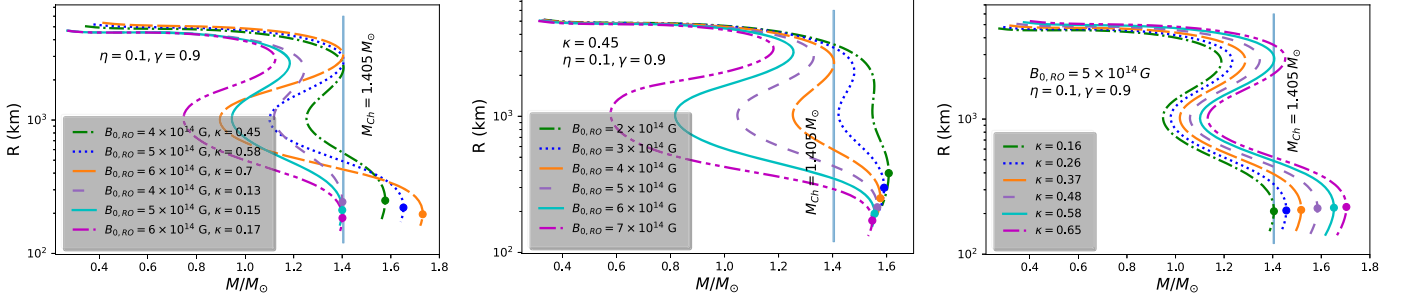

Figure 6. Stellar radius (R) as a function on gravitational mass ($M/M_\odot$) for varying (a) $B_{0,\mathrm{RO}}$ and κ (left panel), (b) $B_{0,\mathrm{RO}}$ (middle panel), and (c) κ (right panel). Solid circles represent the stars with the maximum possible masses.
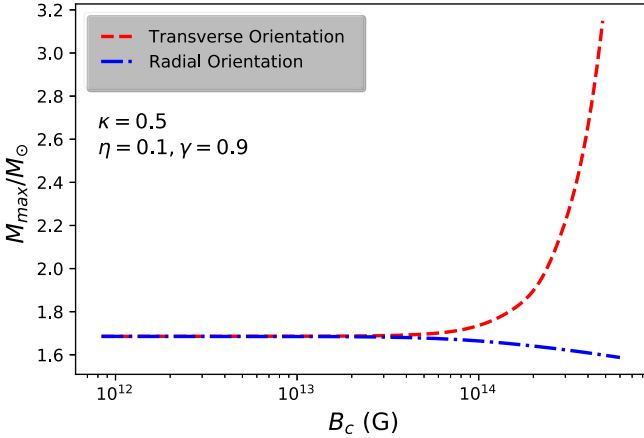
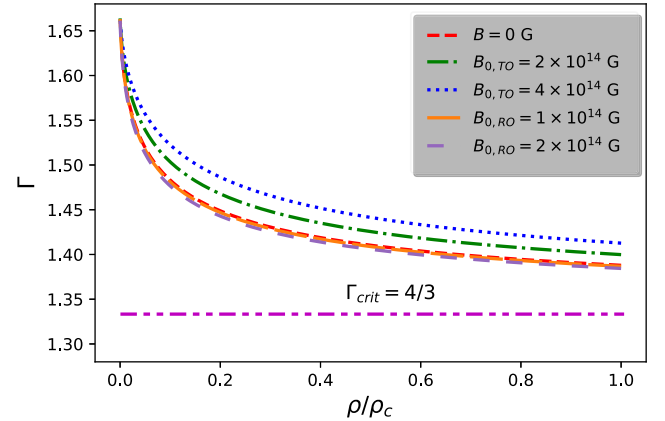**Figure 7.** Variation of stellar mass ($M/M_\odot$) with the central magnetic field (B_c).

Figure 9. Variation of the adiabatic index (Γ) with radial coordinate (r/R) of a $1.3\,M_\odot$ magnetized WD model.
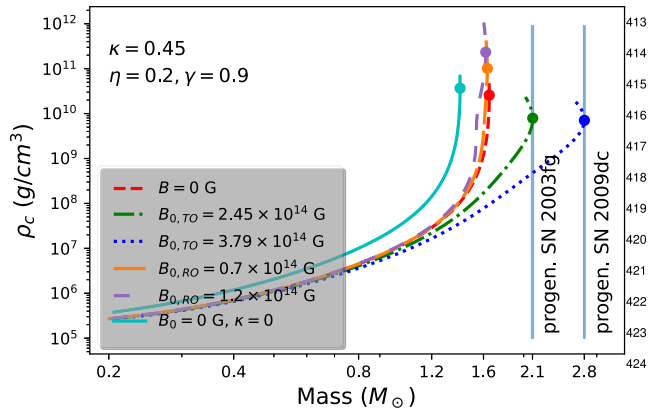

Figure 8. Variation of the central mass density (ρ_c) with stellar mass ($M/M_\odot$). Solid circles represent stars with maximum possible masses.
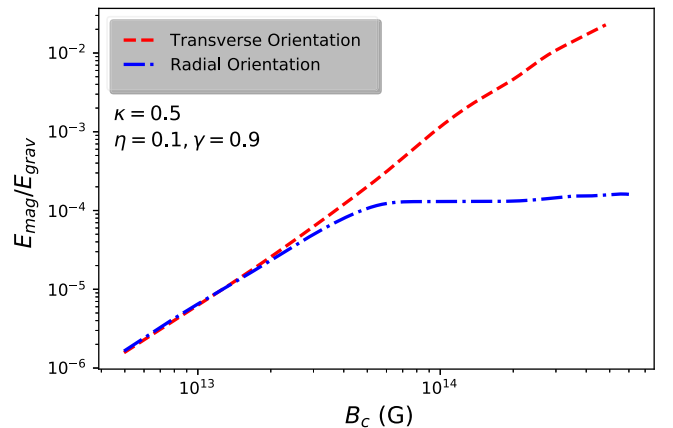

Figure 10. Variation of the ratio of the magnetic energy (E_{mag}) to gravitational energy (E_{grav}) with the central magnetic field (B_c).

Table 1
Physical Parameters of WDs with $B_s = 10^9$ G, $\kappa = 0.45$, $\eta = 0.2$, and $\gamma = 0.9$ for Different B_0

Orientation of Magnetic Field	B_0 (G)	Maximum Mass ($M_\odot$)	Corresponding Predicted Radius (km)	Central Magnetic Field B_c (G)	Central Density $\tilde{\rho}_c$ (g cm^{-3})	Central Pressure $\tilde{p}_c$ (dyne cm^{-2})	$\frac{E_{mag}}{E_{grav}}$
Transverse Orientation	3.79×10^{14}	2.80	1457.67	2.606×10^{14}	7.079×10^9	2.398×10^{28}	1.48×10^{-2}
	2.45×10^{14}	2.10	1357.96	1.772×10^{14}	7.903×10^9	3.389×10^{28}	6.70×10^{-3}
No Magnetic Field	⋯	1.65	927.90	⋯	2.569×10^{10}	9.865×10^{28}	⋯
Radial Orientation	0.7×10^{14}	1.63	601.27	0.7×10^{14}	1.015×10^{11}	1.565×10^{30}	6.04×10^{-5}
	1.2×10^{14}	1.62	454.67	1.2×10^{14}	2.328×10^{11}	5.344×10^{30}	7.75×10^{-5}

Table 2
Physical Parameters of WDs with $B_0 = 3.79 \times 10^{14}$ G, $B_s = 10^9$ G, $\eta = 0.2$, and $\gamma = 0.9$ for Different κ

κ	Maximum Mass ($M_\odot$)	Corresponding Predicted Radius (km)	Central Magnetic Field B_c (G)	Central Density $\tilde{\rho}_c$ (g cm^{-3})	Central Pressure $\tilde{p}_c$ (dyne cm^{-2})	$\frac{E_{mag}}{E_{grav}}$
0	2.36	1443.23	2.812×10^{14}	8.380×10^9	2.867×10^{28}	1.66×10^{-2}
0.15	2.49	1447.92	2.744×10^{14}	7.922×10^9	2.852×10^{28}	1.63×10^{-2}
0.30	2.63	1452.73	2.676×10^{14}	7.488×10^9	2.837×10^{28}	1.55×10^{-2}
0.45	2.80	1457.67	2.606×10^{14}	7.079×10^9	2.823×10^{28}	1.48×10^{-2}

Table 3
Physical Parameters of WDs with $B_0 = 3.79 \times 10^{14}$ G, $B_s = 10^9$ G, and $\kappa = 0.45$ for Different η and γ

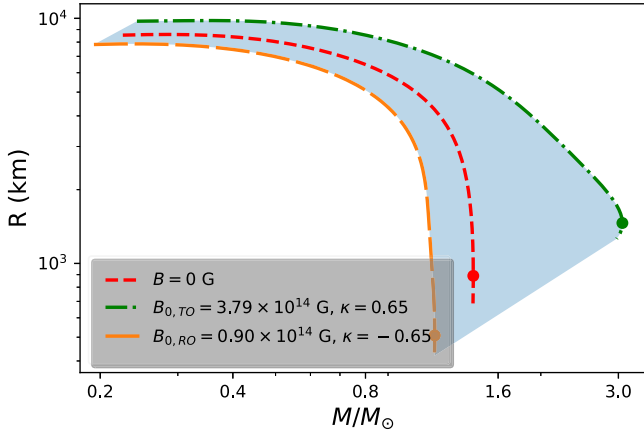| γ and η	Maximum mass ($M_\odot$)	Corresponding Predicted radius (km)	Central Magnetic Field B_c (G)	Central Density $\tilde{\rho}_c$ (g cm^{-3})	Central Pressure $\tilde{p}_c$ (dyne cm^{-2})	$\frac{E_{mag}}{E_{grav}}$
$\gamma = 0.6$, $\eta = 0.1$	1.92	2815.92	6.077×10^{13}	8.610×10^8	1.958×10^{27}	1.62×10^{-1}
$\gamma = 0.7$, $\eta = 0.13$	2.07	1807.05	1.364×10^{14}	3.603×10^9	5.820×10^{27}	3.79×10^{-2}
$\gamma = 0.8$, $\eta = 0.16$	2.33	1488.71	2.528×10^{14}	6.646×10^9	1.815×10^{28}	1.90×10^{-2}
$\gamma = 0.9$, $\eta = 0.2$	2.80	1457.67	2.606×10^{14}	7.079×10^9	2.823×10^{28}	1.48×10^{-2}

Figure 11. Variation of the radius (R) with stellar mass ($M/M_\odot$). Solid circles represent maximum possible stars.

shows that as the free parameter κ increases for a fixed $B_{0,\mathrm{TO}} = 3.79 \times 10^{14}$ G, the maximum masses of the WDs increase. Further, with increasing η and γ for the TO field case, the mass of anisotropic B-WDs changes significantly, as can be seen in the right panel of Figure 5. It shows that the maximum mass of a B-WD with $\gamma = 0.9$ and $\eta = 0.2$ increases by ~46% compared to $\gamma = 0.6$ and $\eta = 0.1$.

Although the inclusion of rotation can explain SCPWD up to 1.7 $M_\odot$, the combined effects of the magnetic field and rotation on WDs can push the maximum mass to much higher values.

However, all these models cannot simultaneously explain sub-Chandrasekhar progenitor WDs. In fact, except for the model proposed by Das & Mukhopadhyay (2015b) and Kalita & Mukhopadhyay (2018), in the realm of modified gravity, no other model can simultaneously explain both the super- and sub-Chandrasekhar WDs to date. Importantly, in this work for RO fields we are able to explain sub-, standard-, and super-Chandrasekhar B-WDs by making appropriate choices of $B_{0,\mathrm{RO}}$ and κ (see Figure 6). By changing both $B_{0,\mathrm{RO}}$ and κ, as shown in the left panel of Figure 6, we successfully explain both (i) the sub- and standard-Chandrasekhar progenitor B-WDs and (ii) the standard and super-Chandrasekhar progenitor B-WDs, by a single mass–radius curve for the respective cases. On the other hand, through changes of only $B_{0,\mathrm{RO}}$ or κ, sub-, standard-, and super-Chandrasekhar B-WDs line up in a series of mass–radius curves, as shown in the middle and right panels of Figure 6. This leads to a complete explanation of under-, regular-, and overluminous SNeIa in a single theory.

From Figure 7 it is evident that the effects of the magnetic field strength on WDs are not the same for the RO and TO magnetic fields, which is the reason for the choice of different B_0 for different field orientations. For example, for a reference value of $B_c = 4 \times 10^{14}$ G and the particular choices $\kappa = 0.5$, $\eta = 0.1$, and $\gamma = 0.9$, the asymmetry between the maximum masses obtained for the RO and TO fields is 65.4%, which indicates how significant the influence of the magnetic field orientations is on WDs. Interestingly, with the increase of $B_{0,\mathrm{TO}}$ the maximum mass, M_{max}, of B-WDs increases rapidly,

whereas the decrease of M_{max} for increasing $B_{0,RO}$ turns out to be not very significant, as shown in Figure 7.

To present a stable, spherically symmetric stellar model, the model must be consistent with the inequality $dM/d\rho_c > 0$ (Harrison et al. 1965) up to its maximum mass for a mass–radius relation. This stability criterion is well satisfied in this work up to the maximum mass star, as shown in Figure 8. To ensure dynamical stability of spherically symmetric compact stars against an infinitesimal radial adiabatic oscillation, Chandrasekhar (1964a, 1964b) introduced a classic technique based on the adiabatic index (Γ) of the system. This result was later revisited and reinstated by Heintzmann & Hillebrandt (1975) who showed that even anisotropic spherically symmetric compact stars should maintain $\Gamma > 4/3$ at all the interior points of the stars to ensure dynamical stability of the stellar structure. We show in Figure 9 that our model is consistent with $\Gamma > 4/3$ at all the interior points of B-WDs. However, Chandrasekhar & Fermi (1953) showed that although it is necessary to be consistent with $\Gamma > 4/3$, which is not sufficient to ensure dynamical stability for the spherically symmetric magnetized compact stars as the presence of a sufficiently strong magnetic field may lead to instability within the stellar structure. They showed that to achieve dynamical stability a spherically symmetric magnetized stellar structure further needs to be consistent with the stability criteria $|E_{grav}| > E_{mag}$, where $|E_{grav}|$ denotes the gravitational potential energy and E_{mag} represents the magnetic energy. Through Figure 10 we show that $|E_{grav}|$ significantly overpowers E_{mag}, which confirms the dynamical stability of the proposed B-WD models.

We show in Tables 1–3 how the combined effects of anisotropy, magnetic field strength, and its orientations have noteworthy influence on the different physical parameters of B-WDs. Table 1 shows the changes of M_{max}, R, B_c, system central density ($\tilde{\rho}_c$), system central pressure ($\tilde{p}_c$), and $|E_{grav}|/E_{mag}$ for varying B_0, where we have chosen $\kappa = 0.45$, $\eta = 0.2$, and $\gamma = 0.9$. In Table 2, we show the change of the said physical parameters for varying κ. Table 3 shows how the physical properties of B-WDs depend on parameters such as η and γ. Throughout our work we have considered only positive κ. One however can see that our model with negative κ (see Silva et al. 2015, for an exploration of negative κ in neutron stars) for the RO fields can suitably explain sub-Chandrasekhar limiting mass WDs. In Figure 11 we show the mass–radius relations for the lower and upper bounds of κ. Importantly, we can explain any WD that lies within the blue shaded area shown in Figure 11.

4. Conclusion

We have analyzed the combined effects of anisotropy, magnetic field strengths, and field orientations on B-WDs. As already pointed out by Chowdhury & Sarkar (2019), magnetic fields are one of the key reasons for anisotropy within WD stars. These authors proposed a spherically symmetric model for anisotropic WDs without considering the presence of a magnetic field. In a separate study Chu et al. (2014), as well as Paper I, showed that RO and TO fields could reduce and enhance, respectively, the maximum mass of strange quark stars. To the best of our knowledge, we study, for the first time in the literature, the properties of spherically symmetric anisotropic B-WDs. As demonstrated, the effective anisotropy, magnetic field strength, and its orientations have a significant

influence on the properties of strongly magnetized WDs. This work manifests many-fold important outcomes as follows:

(i) Through this work, we show that to maintain hydro-dynamic stability at the stellar core for B-WDs, it is important to consider the combined effects of anisotropy due to the fluid and the magnetic field.

(ii) By choosing an appropriate set of constant free parameters, such as B_0 and κ, it is possible to explain highly massive progenitors of peculiar overluminous SNeIa. This immediately questions the idea that the $1.4\,M_\odot$ WD is related to the standard candle, which is used as an important tool to verify the contemporary idea of accelerated expansion of the universe.

(iii) We are able to explain the possible combinations of (a) sub- and standard-Chandrasekhar progenitor B-WDs, (b) standard- and super-Chandrasekhar progenitor B-WDs, and (c) sub- and super-Chandrasekhar progenitor B-WDs, via a single respective mass–radius relation for these cases.

ORCID iDs

Debabrata Deb ⃝ https://orcid.org/0000-0003-4067-5283
Banibrata Mukhopadhyay ⃝ https://orcid.org/0000-0002-3020-9513
Fridolin Weber ⃝ https://orcid.org/0000-0002-5020-1906

References

Abrikosov, A. A. 1960, Soviet Physics, JTEP, 12, 1254
Bandyopadhyay, D., Chakrabarty, S., & Pal, S. 1997, PhRvL, 79, 2176
Bandyopadhyay, D., Pal, S., & Chakrabarty, S. 1998, JPhG, 24, 1647
Bhattacharya, M., Mukhopadhyay, B., & Mukerjee, S. 2018, MNRAS, 477, 2705
Bocquet, M., Bonazzola, S., Gourgoulhon, E., et al. 1995, A&A, 301, 757
Boshkayev, K., Izzo, L., Rueda Hernandez, J. A., et al. 2013, A&A, 555, A151
Bowers, R. L., & Liang, E. P. T. 1974, ApJ, 188, 657
Branch, D. 2006, Natur, 443, 283
Cao, Y., Johansson, J., Nugent, P. E., et al. 2016, ApJ, 823, 147
Cardall, C. Y., Prakash, M., & Lattimer, J. M. 2001, ApJ, 554, 322
Chandrasekhar, S. 1931, ApJ, 74, 81
Chandrasekhar, S. 1935, MNRAS, 95, 207
Chandrasekhar, S. 1964a, ApJ, 140, 417
Chandrasekhar, S. 1964b, PhRvL, 12, 114
Chandrasekhar, S., & Fermi, E. 1953, ApJ, 118, 116
Chen, W.-C., & Li, X.-D. 2009, ApJ, 702, 686
Chowdhury, S., & Sarkar, T. 2019, ApJ, 884, 95
Chu, P.-C., Chen, L.-W., & Wang, X. 2014, PhRvD, 90, 063013
Cumming, A. 2002, MNRAS, 333, 589
Dalcín, L., Paz, R., Storti, M., & D'Elía, J. 2008, JPDC, 68, 655
Das, U., & Mukhopadhyay, B. 2012a, IJMPD, 21, 1242001
Das, U., & Mukhopadhyay, B. 2012b, PhRvD, 86, 042001

Das, U., & Mukhopadhyay, B. 2013a, PhRvL, 110, 071102
Das, U., & Mukhopadhyay, B. 2014a, MPLA, 29, 1450035
Das, U., & Mukhopadhyay, B. 2014b, JCAP, 06, 050
Das, U., & Mukhopadhyay, B. 2015a, JCAP, 05, 016
Das, U., & Mukhopadhyay, B. 2015b, JCAP, 2015, 045
Das, U., Mukhopadhyay, B., & Rao, A. R. 2013b, ApJL, 767, L14
Deb, D., Mukhopadhyay, B., & Weber, F. 2021, ApJ, 992, 149
Dexheimer, V., Franzon, B., Gomes, R. O., et al. 2017, PhLB, 773, 487
Federbush, P., Luo, T., & Smoller, J. 2015, Archive Rational Mech. Analysis, 215, 611
Ferrario, L., Wickramasinghe, D., & Kawka, A. 2020, AdSpR, 66, 1025
Ferrer, E. J., de La Incera, V., Keith, J. P., Portillo, I., & Springsteen, P. L. 2010, PhRvC, 82, 065802
Franzon, B., & Schramm, S. 2015, PhRvD, 92, 083006
Franzon, B., & Schramm, S. 2017, MNRAS, 467, 4484
Frieben, J., & Rezzolla, L. 2012, MNRAS, 427, 3406
Fujisawa, K., Yoshida, S., & Eriguchi, Y. 2012, MNRAS, 422, 434
Garcia-Berro, E., Hernanz, M., Mochkovitch, R., et al. 1988, A&A, 193, 141
Goldhaber, G., Groom, D. E., Kim`, A., et al. 2001, ApJ, 558, 359
Gupta, A., Mukhopadhyay, B., & Tout, C. A. 2020, MNRAS, 496, 894
Harrison, B. K., Thorne, K. S., Wakano, M., et al. 1965, Gravitation Theory and Gravitational Collapse, Vol. 1965 (Chicago: Univ. of Chicago Press)
Heintzmann, H., & Hillebrandt, W. 1975, A&A, 38, 51
Herrera, L., & Barreto, W. 2013, PhRvD, 88, 084022
Hicken, M., Garnavich, P. M., Prieto, J. L., et al. 2007, ApJL, 669, L17
Howell, D. A., Sullivan, M., Nugent, P. E., et al. 2006, Natur, 443, 308
Hunter, J. D. 2007, CSE, 9, 90
Iben, I., & Tutukov, A. V. 1984, ApJS, 54, 335
Ioka, K., & Sasaki, M. 2004, ApJ, 600, 296
Isayev, A. A., & Yang, J. 2011, PhRvC, 84, 065802
Isayev, A. A., & Yang, J. 2012, PhLB, 707, 163
Kalita, S., & Mukhopadhyay, B. 2018, JCAP, 09, 007
Kalita, S., & Mukhopadhyay, B. 2019, MNRAS, 490, 2692
Kalita, S., Mukhopadhyay, B., Mondal, T., & Bulik, T. 2020, ApJ, 896, 69
Kawai, S., Saio, H., & Nomoto, K. 1987, ApJ, 315, 229
Kepler, S. O., Pelisoli, I., Koester, D., et al. 2015, MNRAS, 446, 4078
Kirzhnits, D. A. 1960, Soviet Physics, JTEP, 38, 503, http://jetp.ras.ru/cgi-bin/dn/e_011_02_0365.pdf
Kiuchi, K., & Kotake, K. 2008, MNRAS, 385, 1327
Kiuchi, K., Kotake, K., & Yoshida, S. 2009, ApJ, 698, 541
Kluyver, T., Ragan-Kelley, B., Pérez, F., et al. 2016, in Positioning and Power in Academic Publishing: Players, Agents and Agendas, ed. F. Loizides & B. Schmidt (Amsterdam: IOS Press), 87
Konno, K., Obata, T., & Kojima, Y. 1999, A&A, 352, 211
Kundu, A., & Mukhopadhyay, B. 2012, MPLA, 27, 1250084
Martin, R. G., Tout, C. A., & Lesaffre, P. 2006, MNRAS, 373, 263
Moussa, M. 2017, AnPhy, 385, 347
Mukhopadhyay, B., & Rao, A. R. 2016, JCAP, 2016, 007
Mukhopadhyay, B., Rao, A. R., & Bhatia, T. S. 2017, MNRAS, 472, 3564
Mukhopadhyay, B., Sarkar, A., & Tout, C. A. 2021, MNRAS, 500, 763
Nag, N., & Chakrabarty, S. 2000, arXiv:astro-ph/0008477
Nomoto, K. 1984, ApJ, 277, 791
Nomoto, K. 1987, ApJ, 322, 206
Nomoto, K., & Iben, I., Jr. 1985, ApJ, 297, 531
Nomoto, K., & Kondo, Y. 1991, ApJL, 367, L19
O'Brien, S., & Synge, J. L. 1952, Jump Conditions at Discontinuities in General Relativity, in Communications of the Dublin Institute for Advanced Studies (Dublin)
Oliphant, T. E. 2006, A guide to NumPy, Vol. 1 (USA: Trelgol Publishing)
Oppenheimer, J. R., & Volkoff, G. M. 1939, PhRv, 55, 374
Oron, A. 2002, PhRvD, 66, 023006
Perlmutter, S., Aldering, G., Goldhaber, G., et al. 1999, ApJ, 517, 565
Phillips, M. M. 1993, ApJL, 413, L105
Potter, A. T., & Tout, C. A. 2010, MNRAS, 402, 1072
Quentin, L. G., & Tout, C. A. 2018, MNRAS, 477, 2298
Riess, A. G., Filippenko, A. V., Challis, P., et al. 1998, AJ, 116, 1009
Robson, E. H. 1972, Annales de l'I.H.P. Physique théorique, 16, 41
Roy, S. K., Mukhopadhyay, S., Lahiri, J., & Basu, D. 2019, PhRvD, 100, 063008
Saio, H., & Nomoto, K. 1985, A&A, 150, L21
Saio, H., & Nomoto, K. 1998, ApJ, 500, 388
Saio, H., & Nomoto, K. 2004, ApJ, 615, 444
Salpeter, E. E. 1961, ApJ, 134, 669
Scalzo, R. A., Aldering, G., Antilogus, P., et al. 2010, ApJ, 713, 1073
Schmidt, G. D., Harris, H. C., Liebert, J., et al. 2003, ApJ, 595, 1101
Shah, H., & Sebastian, K. 2017, ApJ, 843, 131
Silva, H. O., Macedo, C. F. B., Berti, E., et al. 2015, CQGra, 32, 145008
Sinha, M., Mukhopadhyay, B., & Sedrakian, A. 2013, NuPhA, 898, 43
Sotani, H., & Tatsumi, T. 2017, MNRAS, 467, 1249
Stevenson, D. J. 1980, JPhys, 41, C2
Subramanian, S., & Mukhopadhyay, B. 2015, MNRAS, 454, 752
Taubenberger, S., Benetti, S., Childress, M., et al. 2011, MNRAS, 412, 2735
Timmes, F. X., Woosley, S. E., & Taam, R. E. 1994, ApJ, 420, 348
Tolman, R. C. 1939, PhRv, 55, 364
Van Der Walt, S., Colbert, S. C., & Varoquaux, G. 2011, CSE, 13, 22
Van Rossum, G., & Drake, F. L. 2009, Python 3 Reference Manual (Scotts Valley, CA: CreateSpace)
Vennes, S., Nemeth, P., Kawka, A., et al. 2017, Sci, 357, 680
Virtanen, P., Gommers, R., Oliphant, T. E., et al. 2020, Nature Methods, 17, 261
Wickramasinghe, D. T., Tout, C. A., & Ferrario, L. 2014, MNRAS, 437, 675
Yasutake, N., Kiuchi, K., & Kotake, K. 2010, MNRAS, 401, 2101
Yoshida, S., Kiuchi, K., & Shibata, M. 2012, PhRvD, 86, 044012